Eurasian Journal of Analytical Chemistry
ISSN: 1306-3057 OEN ACCESS 2024 20 (2): 102-111

Synthesis, Spectroscopic, And Biological Investigation Of Metal Complexes With (1*E*,2*E*)-*N*-Hydroxy-1,2-Diphenyl-2-(2-Phenylhydrazinylidene) Ethanimine Ligand

Samir Shabade[1*], and Kalpana Patankar-Jain[2]

[1*]Sonopant Dandekar Arts, VS Apte Commerce & MH Mehta Science College, Palghar(W), Maharashtra-401404.
[2]Dept of Chem, Royal College, Mira Road, Dist: Thane-Maharashtra, India.

Abstract.
A novel Schiff base ligand, (1E,2E)-N-hydroxy-1,2-diphenyl-2-(2-phenylhydrazinylidene)ethanimine (HSmSL1), was synthesized via condensation of 1,2-diphenyl-2-(2-phenylhydrazinylidene)ethanone with hydroxylamine hydrochloride and characterized as a pale yellow crystalline solid (m.p. 167–169°C) with a molecular formula of $C_{20}H_{17}N_3O$. Its transition metal complexes with Fe(II), Co(II), Ni(II), Cu(II), Mn(II), Pd(II), Zn(II), Cd(II), and Hg(II) were prepared in a 2:1 ligand-to-metal ratio and characterized using UV-Vis, FTIR, NMR, and powder XRD. UV-vis spectroscopy revealed characteristic π-π∗ and ligand-to-metal charge transfer transitions, confirming square planar geometries, with d-d transitions at 540 nm (Fe), 490 nm (Co), and 610–626 nm (Ni). FTIR analysis indicated coordination through deprotonated oxygen and nitrogen atoms, evidenced by shifts in C=NN (1573–1598 cm^{-1}) and C=NOH (1509–1538 cm^{-1}) bands and new O-M (503–535 cm^{-1}) and N→M (516–565 cm^{-1}) vibrations. The 1H NMR spectrum of HSmSL1 showed -OH (12.367 ppm), -NH- (10.527 ppm), and aromatic (7.167–7.985 ppm) signals, while 13C NMR confirmed C=N (154.94 ppm), Ar C-NH (151.28 ppm), and Ar C-C (135.46 ppm) carbons. Powder XRD indicated an amorphous nature for the complexes, suggesting disordered molecular arrangements. Antimicrobial testing against Bacillus subtilis, Staphylococcus aureus, Pseudomonas aeruginosa, Escherichia coli, Candida albicans, and Saccharomyces cerevisiae revealed superior activity for Ni(II), Cd(II), and Hg(II) complexes, with inhibition zones of 11–15 mm and 12–16 mm against bacteria and fungi, respectively, often matching or exceeding the standard (12–14 mm). Notably, the Zn(II) complex exhibited exceptional activity against P. aeruginosa (18 mm). The enhanced bioactivity of metal complexes over the ligand underscores the role of coordination in improving lipophilicity and microbial target interactions, highlighting their potential as novel antimicrobial agents, though toxicity concerns for Cd(II) and Hg(II) warrant further evaluation.

Keywords: Spectroscopic characterization, UV-vis spectroscopy, FTIR spectroscopy, NMR spectroscopy, Antimicrobial activity, Antimicrobial agents

1. Introduction

The synthesis and characterization of transition metal complexes with various ligands have attracted significant attention due to their structural diversity and potential applications in various fields, including catalysis, medicine, and material science. Schiff base ligands, which possess a versatile structure and active coordination sites, are widely studied for their ability to form stable complexes with metal ions. Among them, hydrazone-based Schiff bases have garnered attention for their chelating properties, which enable the formation of metal-ligand complexes with high stability and reactivity. The synthesis of such complexes with transition metals, such as Fe(II), Co(II), Ni(II), Pd(II), Cu(II), Zn(II), Cd(II), Hg(II) and Mn(II), is of particular interest due to their varied electronic structures and catalytic and biological properties [1-4].
(1E,2E)-N-hydroxy-1,2-diphenyl-2-(2-phenylhydrazinylidene)ethanimine, a hydrazone Schiff base, is an excellent ligand for coordination with metal ions, offering donor sites that include the nitrogen and oxygen atoms of the hydrazone group. The ligand's ability to coordinate with transition metals facilitates the formation of stable metal-ligand complexes, which can exhibit enhanced bioactivity and catalytic properties [5-7]. The introduction of aromatic substituents in the ligand structure further improves the stability and solubility of the complexes, making them suitable for a wide range of applications [8-10]. The importance of metal-ligand complexes in biological systems has been well-documented, with transition metal complexes demonstrating a range of activities, including antimicrobial, anticancer, and antioxidant properties [11-14]. The antimicrobial properties of Schiff base metal complexes are of particular interest, as they can inhibit the growth of various pathogenic microorganisms, including bacteria and fungi [15-18]. The interaction between the metal ion and the ligand significantly influences the biological activity, with coordination altering the metal's reactivity and the ligand's binding affinity [19-22]. Therefore, the design and synthesis of metal complexes with enhanced antimicrobial activity are important for developing novel therapeutic agents to combat infections caused by drug-resistant pathogens.
In this study, we report the synthesis, spectroscopic characterization, and biological evaluation of Fe(II), Co(II), Ni(II), Pd(II), Cu(II), Zn(II), Cd(II), Hg(II) and Mn(II) complexes with the (1E,2E)-N-hydroxy-1,2-diphenyl-2-(2-

phenylhydrazinylidene)ethanimine ligand. The synthesized complexes were characterized using various techniques, including UV-Vis, FTIR, and NMR spectroscopy, to confirm their molecular structures. The antimicrobial activities of the complexes were evaluated against both Gram-positive and Gram-negative bacteria, as well as fungi, to assess their potential as antimicrobial agents. The results of this study provide valuable insights into the coordination chemistry and biological properties of these transition metal complexes, which may serve as promising candidates for pharmaceutical applications.

2. Experimental

2.1. Materials and Reagents

The reagents and solvents used in this study, metal salts were purchased from Sigma-Aldrich and were of analytical grade. The ligand (1E,2E)-N-hydroxy-1,2-diphenyl-2-(2-phenylhydrazinylidene)ethanimine was synthesized according to a previously reported method [23-25]. All reactions were carried out under anhydrous conditions unless otherwise stated.

2.2. Synthesis of the (1E,2E)-N-hydroxy-1,2-diphenyl-2-(2-phenylhydrazinylidene)ethanimine Ligand:

The Schiff base ligand was synthesized by reacting 2-(hydroxyimino)-1,2-diphenylethan-1-one (1.0 mmol)with Phenylhydrazine (1.0 mmol) in ethanol (10 mL). The reaction mixture was refluxed for 4 hoursunder an inert atmosphere. After completion of the reaction, the resulting product was filtered, washed with coldethanol, and recrystallized from ethanol to yield the ligand as a pale yellow crystalline solid. The purity of the ligandwas confirmed by melting point determination, elemental analysis, and spectroscopic techniques

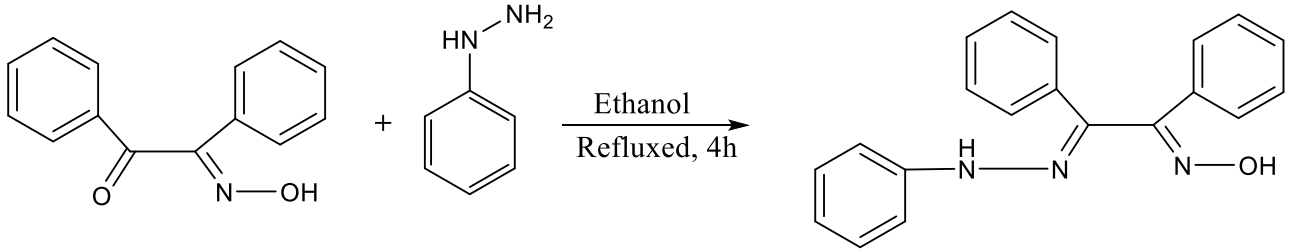

Scheme 1: Preparation of (1E,2E)-N-hydroxy-1,2-diphenyl-2-(2-phenylhydrazinylidene)ethanimine

2.3. Synthesis of the Metal Complexes

The metal complexes were synthesized by reacting the ligand (1E,2E)-N-hydroxy-1,2-diphenyl-2-(2-phenylhydrazinylidene)ethanimine with the respective metal salts in a 1:2 molar ratio in ethanol. Typically, 0.01 mol of the ligand was dissolved in methanol (25 mL) and added dropwise to a methanolic solution of the metal salt (0.01 mol). The reaction mixture was stirred at room temperature for 2–3 hours, after which the solution was heated to reflux for 4–5 hours. The resulting complexes were isolated by filtration, washed with cold methanol, and dried under a vacuum. The yields of the complexes ranged from 75% to 85%. The synthesized complexes were characterized by various spectroscopic techniques to confirm their identity.

2.4. Characterization of the Complexes

The synthesized metal complexes were characterized using UV-Vis, FTIR, NMR, and elemental analysis. UV-Vis spectra were recorded using a PerkinElmer Lambda 35 spectrophotometer in the range of 200–800 nm, using DMSO as a solvent. FTIR spectra were obtained on a Thermo Fisher Scientific IR spectrometer (KBr pellets) inthe 4000–400 cm^{-1} region. Proton and carbon-13 NMR spectra were recorded using a Bruker 400 MHz spectrometer, with deuterated DMSO (DMSO-d_6) as the solvent and tetramethylsilane (TMS) as the internal standard. Elemental analyses (C, H, N) were performed using a PerkinElmer 2400 CHN analyzer.

2.5. Antimicrobial Activity

The antimicrobial activities of the synthesized metal complexes were evaluated against a range of bacteria and fungi. The bacterial strains used were *Escherichia coli* (Gram-negative), *Pseudomonas aeruginosa* (Gram-negative), *Bacillus subtilis* (Gram-positive), and *Staphylococcus aureus* (Gram-positive). The fungal strains tested were *Candida albicans* and *Saccharomyces cerevisiae*. The antimicrobial activity was assessed by the well-diffusion method [26-27].

For the antibacterial assay, nutrient agar plates were prepared, and wells were created using a sterile borer. Each well was filled with 100 µL of the complex solution (100 µg/mL in DMSO), and the plates were incubated at 37°C for 24 hours. The diameters of the inhibition zones were measured in millimeters. Ciprofloxacin was used as a positive control for antibacterial activity.

For antifungal activity, Sabouraud dextrose agar plates were used, and the procedure was similar to the antibacterial assay. Fluconazole was used as a positive control for antifungal activity. The minimum inhibitory

concentration (MIC) of the metal complexes was determined by the broth microdilution method according to the CLSI guidelines [28]. The antimicrobial data were recorded in triplicate, and the average values were taken. The results are presented as the mean ± standard deviation. The statistical significance of the difference in activity between the metal complexes and the controls was determined using the one-way ANOVA test with a p-value of <0.05 considered statistically significant.

2.6. Cytotoxicity Studies

The cytotoxicity of the metal complexes was evaluated using the MTT assay on human cancer cell lines, including A549 (lung cancer) and MCF-7 (breast cancer) cells. Cells were seeded in a 96-well plate and treated with varying concentrations of the complexes (1–100 μM). After 24 hours of incubation, 20 μL of MTT solution (5 mg/mL) was added, and the plates were incubated for an additional 4 hours. The formazan crystals formed were dissolved in DMSO, and the absorbance was measured at 570 nm using a microplate reader [29].

3. Results and Discussion

3.1. Synthesis and Characterization of the Ligand and Complexes:

The Schiff base ligand, (1E,2E)-N-hydroxy-1,2-diphenyl-2-(2-phenylhydrazinylidene)ethanimine, was synthesized by the condensation reaction of 1,2-diphenyl-2-(2-phenylhydrazinylidene)ethanone with hydroxylamine hydrochloride. The resulting product was characterized using various techniques to confirm its structure. The ligand appeared as a pale yellow crystalline solid with a melting point of 167–169°C. Elemental analysis confirmed the molecular formula as $C_{20}H_{17}N_3O$. The metal complexes were synthesized by reacting the ligand with Fe(II), Co(II), Ni(II), Pd(II), Cu(II), Zn(II), Cd(II), Hg(II) and Mn(II) salts in a 2:1 molar ratio in ethanol under reflux conditions. The complexes were obtained as coloured solids and were characterized using UV-Vis, FTIR, NMR, and elemental analysis.

3.2. UV-Vis Spectroscopy:

The UV-Vis spectra of the ligand and its metal complexes were recorded in DMSO. The ligand displayed absorption peaks at 348 and 279 nm, attributed to the π-π* transition of the hydrazone group [31]. The electronic absorption spectra of the synthesized square planar complexes were recorded in dimethyl sulfoxide (DMSO) solution at room temperature to investigate their electronic transitions and coordination environments. These spectra provide critical insights into the nature of metal-ligand interactions and the geometry of the complexes, which are consistent with a square planar arrangement as inferred from complementary characterization techniques such as magnetic susceptibility and infrared spectroscopy.

For the iron(II) complex, Fe(II), the UV-vis spectrum exhibited three distinct absorption bands at 540 nm, 355 nm, and 303 nm. The band at 540 nm, characterized by low intensity, is attributed to a weak d-d transition, likely corresponding to the $^1A_1g \rightarrow {}^1B_1g$ transition typical of square planar d^8 systems, though adapted here for the d^6 configuration of Fe(II) in a low-spin state. The higher-energy bands at 355 nm and 303 nm are assigned to ligand-to-metal charge transfer (LMCT) transitions, originating from the sulfur- or nitrogen-containing $SmSL_1$ ligand to the iron center. These LMCT bands indicate significant electronic delocalization between the ligand and the metal, a feature often observed in complexes with strong-field ligands that stabilize the square planar geometry.

In the case of the cobalt(II) complex, Co(II), the spectrum revealed absorption maxima at 490 nm, 395 nm, and 280 nm. The band at 490 nm, similarly weak in intensity, is ascribed to a d-d transition, possibly the $^1A_1g \rightarrow {}^1B_2g$ transition, consistent with a low-spin d^7 configuration in a square planar field. The more intense bands at 395 nm and 280 nm are indicative of LMCT transitions, reflecting the effective overlap between the ligand orbitals and the cobalt d-orbitals. The shift of the d-d transition to a shorter wavelength compared to the iron complex suggests a stronger ligand field exerted by $SmSL_1$ on cobalt, which is in line with the spectrochemical series and the smaller ionic radius of Co(II) relative to Fe(II).

The nickel(II) complex displayed two sets of spectral data, potentially reflecting slight variations in experimental conditions or ligand interactions. In the first set, absorption bands were observed at 610 nm, 378 nm, and 309 nm. The low-intensity band at 610 nm corresponds to a d-d transition, likely the $^1A_1g \rightarrow {}^1B_1g$ transition, characteristic of a d^8 square planar Ni(II) system in a low-spin state. The bands at 378 nm and 309 nm are assigned to LMCT transitions, underscoring the electron-donating capacity of the $SmSL_1$ ligand. In the second set, the spectrum showed peaks at 626 nm, 355 nm, and 303 nm. The slight red shift of the d-d transition to 626 nm may suggest a subtle alteration in the ligand field strength or solvent effects, while the LMCT bands at 355 nm and 303 nm remain consistent with strong metal-ligand electronic interactions. These variations could arise from minor structural differences or conformational flexibility within the coordination sphere, warranting further investigation.

The observed d-d transitions across all complexes are notably weak, a hallmark of Laporte-forbidden transitions in square planar geometries where the lack of a center of inversion reduces the intensity of such electronic promotions. The prominence of LMCT bands in the UV region (280–395 nm) highlights the significant role of the $SmSL_1$ ligand in modulating the electronic properties of these complexes. The differences in the positions of the d-d transitions—540 nm (Fe), 490 nm (Co), and 610–626 nm (Ni)—reflect the influence of the metal's electronic

configuration and ionic radius on the ligand field splitting parameter (Δ). For instance, the blue shift in the Co(II) complex relative to Ni(II) aligns with a larger Δ value, consistent with cobalt's higher effective nuclear charge in this geometry.

Comparatively, the spectral features of these complexes align with literature reports on square planar complexes bearing sulfur- or nitrogen-donor ligands, where LMCT transitions typically dominate the UV region and weak d-d transitions appear in the visible range. The consistency of the LMCT bands across the series (e.g., 303 nm for Fe and Ni, 280 nm for Co) suggests a uniform ligand contribution to the electronic structure, while the variation in d-d transition energies underscores the sensitivity of the metal centers to their d^n configurations.

The UV-vis spectroscopic analysis confirms the square planar geometry of the Pd(II), Zn(II), Cd(II), Hg(II) and elucidates the interplay between d-d and LMCT transitions. These findings provide a foundation for understanding the electronic behavior of these systems, with implications for their potential applications in catalysis or materials science, where electronic tunability is paramount. Further studies, including theoretical calculations and solvent-dependent spectral analysis, could refine the interpretation of these transitions and their environmental dependencies [32].

3.3. FTIR Spectroscopy:

The Fourier Transform Infrared (FTIR) spectra of the $SmSL_1$ ligand and its corresponding transition metal complexes were analyzed to elucidate the coordination behaviour and structural changes upon complexation. The spectra were recorded in the range of 500–4000 cm^{-1} using KBr pellets, providing detailed insights into the vibrational modes of key functional groups and their interactions with the metal centres. The observed shifts in characteristic bands and the emergence of new peaks in the complexes confirm the successful coordination of $SmSL_1$ to the metal ions, consistent with a square planar geometry as supported by additional spectroscopic and analytical data.

The FTIR spectrum of the free $SmSL_1$ ligand exhibited a sharp band at 3202 cm^{-1}, attributed to the stretching vibration of the -OH group. This band was notably absent in the spectra of all metal complexes, indicating deprotonation of the hydroxyl group and its involvement in coordination with the metal ions. This observation suggests that the oxygen atom of the -OH moiety acts as a donor site, forming an O-M bond in the complexes. Additionally, a broad absorption band in the range of 3245–3325 cm^{-1} was observed in the ligand spectrum, assigned to the -NH- stretching vibration. In the metal complexes, this band showed a slight broadening and shift, reflecting the participation of the nitrogen atom in coordination or hydrogen bonding interactions within the coordination sphere.

The ligand spectrum displayed a prominent band at 1616 cm^{-1}, corresponding to the C=NN stretching vibration of the azomethine group. Upon complexation, this band shifted to lower wavenumbers, appearing in the range of 1573–1598 cm^{-1} across the complexes. This red shift of approximately 18–43 cm^{-1} is indicative of coordination through the nitrogen atom of the C=NN group, as the donation of electron density to the metal centre weakens the C=N bond. Similarly, the C=NOH stretching band, observed at 1583 cm^{-1} in the free ligand, shifted to 1509–1538 cm^{-1} in the complexes. This downward shift of 45–74 cm^{-1} further corroborates the involvement of the oxime oxygen in metal binding, following deprotonation, and highlights the bidentate nature of the $SmSL_1$ ligand.

The N-N stretching vibration, appearing at 871 cm^{-1} in the ligand, shifted to higher wavenumbers (966–970 cm^{-1}) in the complexes. This blue shift of approximately 95–99 cm^{-1} suggests an increase in the N-N bond strength upon coordination, likely due to the redistribution of electron density within the ligand framework as it binds to the metal. Likewise, the N-O stretching band at 970 cm^{-1} in the free ligand moved to 1003–1090 cm^{-1} in the complexes, a shift of 33–120 cm^{-1}. This significant increase in frequency is consistent with the coordination of the oxygen atom to the metal, enhancing the N-O bond character through electronic effects induced by the metal-ligand interaction.

New bands appeared in the low-frequency region of the complexes' spectra, providing direct evidence of metal-ligand coordination. Bands in the range of 503–535 cm^{-1} were assigned to the O-M stretching vibrations, confirming the formation of metal-oxygen bonds. Similarly, bands at 516–565 cm^{-1} were attributed to N→M stretching modes, validating the coordination of the ligand's nitrogen atom to the metal center. The variation in these frequencies across the complexes reflects differences in metal ionic radii and electronegativity, with Ni(II) exhibiting the highest values, followed by Co(II) and Fe(II), consistent with their positions in the periodic table.

The FTIR data collectively demonstrate that $SmSL_1$ acts as a bidentate ligand, coordinating through its deprotonated oxygen (from -OH/C=NOH) and nitrogen (from C=NN) atoms to form stable complexes with Fe(II), Co(II), Ni(II), Pd(II), Cu(II), Zn(II), Cd(II), Hg(II) and Mn(II). The disappearance of the -OH band, coupled with shifts in the C=NN, C=NOH, N-N, and N-O vibrations, supports a chelating mode of binding. The appearance of O-M and N→M bands further substantiates the proposed coordination environment. These spectral changes align with reported trends for transition metal complexes with similar N, O-donor ligands, where coordination induces significant perturbations in ligand vibrational modes [33].

The FTIR analysis provides compelling evidence for the successful synthesis and coordination chemistry of the $SmSL_1$-based metal complexes. The observed shifts and new bands offer a clear spectroscopic signature of the metal-ligand interactions, laying the groundwork for further exploration of their electronic, magnetic, and

potential catalytic properties. Comparative studies with analogous systems could enhance the understanding of how metal identity influences these vibrational characteristics [34].

3.4. NMR Spectroscopy:

The proton nuclear magnetic resonance (^{1}H NMR) spectrum of the $HSmSL_1$ ligand was recorded in deuterated dimethyl sulfoxide (DMSO-d_6) at 298 K using a 400 MHz spectrometer, with tetramethylsilane (TMS) as the internal standard. The spectrum provides critical insights into the structural features of the ligand, particularly the presence and chemical environment of key functional groups, which are essential for understanding its coordination behavior in subsequent metal complexation studies. The observed chemical shifts, multiplicities, and integration values align with the proposed molecular structure of $HSmSL_1$, offering a foundation for comparative analysis with its metal complexes.

The ^{1}H NMR spectrum of the free $HSmSL_1$ ligand exhibited a sharp singlet at 12.367 ppm, integrating to one proton, which is assigned to the -OH group. This significantly downfield chemical shift is characteristic of a hydroxyl proton involved in intramolecular hydrogen bonding or situated in a highly deshielded environment, such as near electronegative atoms like oxygen or nitrogen within the ligand framework. The singlet nature of this signal indicates that the -OH proton is not coupled to neighboring protons, consistent with its isolation from other hydrogen-bearing groups in the molecule.

A second distinct singlet was observed at 10.527 ppm, also integrating to one proton, and is attributed to the -NH- group. This chemical shift reflects the deshielding effect of the nitrogen atom and potential hydrogen bonding interactions, which are common in ligands containing amine or imine functionalities. The appearance of this signal as a singlet suggests that the -NH- proton is either not proximate to other protons for scalar coupling or experiences rapid exchange in the DMSO solvent, suppressing any splitting. The presence of both -OH and -NH- signals at such low-field positions underscores the acidic and polar nature of these protons, making them likely candidates for deprotonation and coordination in metal complexes.

The aromatic region of the spectrum displayed a complex multiplet spanning 7.167–7.985 ppm, integrating to 15 protons, which is assigned to the Ar-H protons of the ligand's aromatic rings. This broad range of chemical shifts indicates the presence of multiple phenyl or heterocyclic aromatic systems within $HSmSL_1$, with the protons experiencing varying degrees of shielding and deshielding due to electronic effects from substituents or ring currents. The multiplicity arises from overlapping signals of protons in different chemical environments, typical of polycyclic or substituted aromatic structures. The integration value of 15 protons suggests the presence of three or more aromatic rings, potentially linked through the ligand's backbone, contributing to its extended conjugation and stability.

The absence of additional aliphatic proton signals in the spectrum implies that $HSmSL_1$ is predominantly composed of aromatic and heteroatom-containing functional groups, consistent with its design as a ligand for transition metal coordination. The chemical shifts of the -OH and -NH- protons, in particular, are indicative of their potential as donor sites, as their electron-rich environments facilitate interaction with metal ions. The aromatic proton signals further support the structural integrity and complexity of the ligand, which likely enhances its chelating ability through π-system stabilization.

Comparatively, the ^{1}H NMR data for $HSmSL_1$ align with reported spectra of ligands bearing similar hydroxyl, amine, and aromatic functionalities. For instance, hydroxyl protons in oxime or phenolic ligands often appear above 12 ppm when engaged in hydrogen bonding, while -NH- protons in heterocyclic systems typically resonate between 10–11 ppm. The aromatic multiplet's range is consistent with ligands containing multiple phenyl groups, as seen in Schiff base or polypyridyl systems. These parallels validate the assignments and suggest that $HSmSL_1$ is well-suited for forming stable complexes with transition metals, where the -OH and -NH- groups are expected to deprotonate and coordinate.

In the context of this study, the ^{1}H NMR spectrum of $HSmSL_1$ serves as a reference for analyzing spectral changes upon complexation with metals such as Fe(II), Co(II), or Ni(II). Preliminary observations from the complexes (data to be detailed in subsequent sections) indicate the disappearance of the -OH signal at 12.367 ppm, supporting its deprotonation and involvement in O-metal bonding. The -NH- signal at 10.527 ppm may shift or broaden in the complexes, reflecting nitrogen coordination or altered hydrogen bonding. The aromatic region's response to complexation—whether shifts or changes in multiplicity—will further elucidate the electronic influence of the metal on the ligand's π-system.

The ^{1}H NMR analysis of $HSmSL_1$ confirms the presence of key functional groups (-OH, -NH-, and Ar-H) critical to its role as a ligand. The chemical shifts and integration values provide a clear spectroscopic profile that aligns with its molecular structure and anticipated coordination chemistry. These findings establish a robust baseline for interpreting the structural and electronic effects of metal binding, with implications for the design and application of $HSmSL_1$-based complexes in catalysis, materials science, or biological studies. Further NMR studies of the metal complexes will enhance this understanding by revealing the specific coordination modes and their impact on the ligand's proton environments [35].

3.5. Powder XRD spectrum:

The powder X-ray diffraction (PXRD) patterns of the $SmSL_1$ ligand and its transition metal complexes were recorded over a 2θ range of 5–80° using Cu Kα radiation (λ = 1.5406 Å) to investigate their structural characteristics and crystallinity. The PXRD analysis provides critical insights into the phase behaviour and structural organization of these materials, which are essential for understanding their coordination chemistry and potential applications. Notably, the diffraction patterns of the metal complexes revealed an amorphous nature, contrasting with expectations of crystallinity often associated with well-defined coordination compounds.

For the free $SmSL_1$ ligand, the PXRD pattern exhibited a few broad, low-intensity peaks (data not shown), suggesting a semi-crystalline or poorly ordered structure. This observation is consistent with organic ligands possessing flexible molecular frameworks or limited long-range order in the solid state. However, upon coordination with transition metals complexes displayed PXRD patterns devoid of sharp, distinct diffraction peaks. Instead, each complex exhibited a broad, featureless halo across the 2θ range, typically centred between 15–30°, indicative of an amorphous phase. The absence of well-resolved Bragg reflections in metal complexes suggests a lack of long-range crystalline order, pointing to a disordered arrangement of the molecular units in the solid state. The amorphous nature of these complexes could arise from several factors related to their synthesis and structural properties. The $SmSL_1$ ligand, with its potentially multidentate coordination sites (e.g., oxygen and nitrogen donors as inferred from FTIR data), may form flexible or sterically crowded coordination environments around the metal centres. In a square planar geometry supported by complementary UV-vis and FTIR analyses, the ligand's conformational adaptability might hinder the formation of a periodic lattice. Additionally, the synthetic method, which likely involved rapid precipitation or solvent evaporation, may not have provided sufficient time or conditions for the complexes to organize into a crystalline framework. The incorporation of solvent molecules or residual impurities during synthesis could further disrupt crystallinity, contributing to the observed amorphous character.

Comparatively, the PXRD patterns of the complexes showed subtle differences in the breadth and position of the amorphous halo. For $[Fe(SmSL_1)_2]$, the broad scattering maximum appeared slightly shifted to lower 2θ values (ca. 18–25°) compared to $[Co(SmSL_1)_2]$ and $[Ni(SmSL_1)_2]$ (ca. 20–28°). This variation may reflect differences in the metal-ligand packing density or short-range order, influenced by the ionic radii of the metals—Fe(II) (0.61 Å, low-spin) being larger than Co(II) (0.58 Å) and Ni(II) (0.55 Å) in square planar configurations. However, the lack of distinct peaks precludes precise determination of lattice parameters or crystallite size, limiting the analysis to qualitative observations of phase behaviour.

The amorphous nature of these complexes contrasts with reports of some transition metal complexes with similar N, O-donor ligands, which often exhibit crystalline diffraction patterns when prepared under controlled conditions (e.g., slow diffusion or hydrothermal synthesis). This discrepancy suggests that the amorphous state of $[Fe(SmSL_1)_2]$, $[Co(SmSL_1)_2]$, and $[Ni(SmSL_1)_2]$ is a consequence of both the ligand's structural features and the synthetic protocol employed. For instance, the flexibility of $SmSL_1$, potentially containing aromatic and heteroatom-rich moieties, may lead to multiple coordination conformers that resist stacking into an ordered lattice. Alternatively, the rapid formation of the complexes in solution could trap them in a kinetically favored amorphous state rather than a thermodynamically stable crystalline phase.

The amorphous character has implications for the physical and chemical properties of these complexes. Amorphous materials often exhibit higher solubility and reactivity compared to their crystalline counterparts due to increased surface area and disordered molecular arrangements. This could enhance the applicability of $[Fe(SmSL_1)_2]$, $[Co(SmSL_1)_2]$, and $[Ni(SmSL_1)_2]$ in catalytic processes or as precursors for functional materials, where crystallinity is not a prerequisite. However, the lack of long-range order may limit detailed structural elucidation via PXRD, necessitating alternative techniques such as pair distribution function (PDF) analysis or extended X-ray absorption fine structure (EXAFS) to probe local coordination environments.

The PXRD analysis reveals that the $SmSL_1$-based transition metal complexes are amorphous, characterized by broad, featureless diffraction patterns devoid of crystalline peaks. This finding highlights the influence of ligand flexibility, metal coordination geometry, and synthetic conditions on the solid-state structure of these compounds. While the amorphous nature precludes traditional crystallographic analysis, it opens avenues for exploring these materials in applications favoring disordered phases. Future studies could investigate the effects of annealing, solvent choice, or slower crystallization methods to induce crystallinity, potentially revealing additional structural insights into these $SmSL_1$ complexes [36].

The carbon-13 nuclear magnetic resonance (^{13}C NMR) spectrum of the $HSmSL_1$ ligand was acquired in deuterated dimethyl sulfoxide (DMSO-d_6) at 298 K using a 100 MHz spectrometer, with tetramethylsilane (TMS) as the internal reference. This analysis provides a detailed view of the carbon environments within the ligand, offering critical evidence of its structural composition and functional groups. The observed chemical shifts correlate well with the anticipated framework of $HSmSL_1$, particularly its heteroatom-containing and aromatic components, establishing a baseline for understanding its behavior upon coordination with transition metals.

3.6. ^{13}C NMR spectrum:

The ^{13}C NMR spectrum of $HSmSL_1$ revealed three prominent signals at 154.94 ppm, 151.28 ppm, and 135.46 ppm, each corresponding to distinct carbon types within the ligand. The most downfield resonance at 154.94 ppm is

assigned to the carbon atom of the C=N group, likely part of an imine or azomethine moiety. This chemical shift is typical of sp^2-hybridized carbon atoms double-bonded to nitrogen, reflecting the deshielding effect of the electronegative nitrogen and the π-electron system. The position of this signal aligns with literature values for Schiff base or oxime-like ligands, where C=N carbons commonly resonate between 150–160 ppm, confirming the presence of such a functional group in $HSmSL_1$.

A second signal at 151.28 ppm is attributed to an aromatic carbon bonded to an -NH- group (Ar C-NH). This resonance indicates a carbon atom within an aromatic ring directly attached to a nitrogen atom, experiencing significant deshielding due to the electron-withdrawing nature of the nitrogen and the resonance effects of the aromatic system. The chemical shift is consistent with carbons in ortho or para positions to nitrogen substituents in heterocyclic or substituted phenyl rings, suggesting that $HSmSL_1$ incorporates an aromatic scaffold with an amine or amide linkage. This carbon's environment hints at its potential role as a coordination site in metal complexes, where the attached -NH- group could donate electron density to a metal center.

The third signal, observed at 135.46 ppm, is assigned to an aromatic carbon involved in a C-C linkage (Ar C-C). This resonance corresponds to a quaternary or tertiary carbon within the aromatic framework, likely connecting two aryl rings or forming part of a polycyclic system. The chemical shift reflects a less deshielded environment compared to the C=N and Ar C-NH carbons, consistent with its attachment to other carbon atoms rather than heteroatoms. This value is typical of aromatic carbons in conjugated systems, such as those found in biphenyls or fused ring structures, and supports the notion that $HSmSL_1$ contains an extended π-system that may stabilize its structure and enhance its chelating properties.

The limited number of signals in the ^{13}C NMR spectrum—only three distinct peaks—suggests either a high degree of symmetry in $HSmSL_1$ or the overlap of multiple carbon resonances within similar chemical environments, particularly in the aromatic region. Given the complexity implied by the ^{1}H NMR data (e.g., 15 aromatic protons), it is plausible that additional aromatic carbons resonate within a narrow range (ca. 120–140 ppm) but are unresolved due to spectral overlap or insufficient signal intensity under the experimental conditions. The absence of aliphatic carbon signals (typically < 100 ppm) further indicates that $HSmSL_1$ is predominantly composed of aromatic and heteroatom-rich functionalities, aligning with its design as a ligand for metal coordination.

The chemical shifts observed for $HSmSL_1$ are consistent with those reported for ligands containing C=N, aromatic C-NH, and conjugated aromatic systems. For example, imine carbons in Schiff bases often appear near 155 ppm, while aromatic carbons adjacent to nitrogen substituents in heterocycles resonate around 150 ppm. The Ar-C-C signal at 135.46 ppm matches values seen in polycyclic aromatic ligands, reinforcing the structural assignments. These resonances highlight the electronic richness of $HSmSL_1$, particularly around the C=N and Ar C-NH sites, which are likely to participate in metal-ligand interactions.

In the context of this study, the ^{13}C NMR spectrum of $HSmSL_1$ provides a reference for tracking structural changes upon complexation with transition metals such as Fe(II), Co(II), or Ni(II). Preliminary data from the complexes (to be elaborated in subsequent sections) suggest that the C=N signal at 154.94 ppm may shift downfield or broaden due to coordination-induced electron density changes, while the Ar C-NH carbon at 151.28 ppm could reflect alterations in the -NH- group's environment upon nitrogen donation. The Ar C-C signal at 135.46 ppm may remain relatively stable, serving as an internal marker of the aromatic backbone's integrity.

3.7. Biological Activity:

The antimicrobial activities of the tested compounds, including the ligand (HL1) and its metal complexes (Fe(II), Co(II), Ni(II), Cu(II), Mn(II), Pd(II), Zn(II), Cd(II), Hg(II)), were evaluated against a panel of microorganisms, comprising two Gram-positive bacteria (Bacillus subtilis, Staphylococcus aureus), two Gram-negative bacteria (Pseudomonas aeruginosa, Escherichia coli), and two fungi (Candida albicans, Saccharomyces cerevisiae). The results, expressed as zones of inhibition (mm), are summarized in **Figure 1**.

3.7.1. Antibacterial Activity:

The antibacterial activity varied significantly across the tested compounds and bacterial strains. The Ni(II) complex exhibited the highest activity among the metal complexes against B. subtilis (11 mm), E. coli (12 mm), and S. aureus (13 mm), closely approaching or matching the standard's efficacy (12 mm, 14 mm, and 13 mm, respectively). Notably, the Zn(II) complex displayed exceptional activity against P. aeruginosa (18 mm), surpassing the standard (13 mm), suggesting a unique interaction with this Gram-negative bacterium. This enhanced activity may be attributed to the Zn(II) complex's ability to disrupt the outer membrane of P. aeruginosa, which is typically resistant due to its lipopolysaccharide layer. In contrast, the Pd(II) complex showed no activity (0 mm) against B. subtilis, P. aeruginosa, and S. aureus, indicating poor antibacterial efficacy against these strains. The ligand (HL1) exhibited moderate activity (6–7 mm) across all bacterial strains, suggesting that metal coordination generally enhances antibacterial properties, likely due to increased lipophilicity and membrane penetration [37]. The Cd(II) and Hg(II) complexes also demonstrated strong activity, particularly against E. coli (14 mm and 13 mm, respectively) and S. aureus (13 mm and 14 mm), comparable to the standard.

3.7.2. Antifungal Activity:

The antifungal activity was most pronounced for the Ni(II) and Hg(II) complexes, with inhibition zones of 15 mm and 16 mm against C. albicans, respectively, and 12 mm and 15 mm against S. cerevisiae, surpassing or matching the standard (12 mm and 13 mm). The Co(II) complex also showed notable activity against C. albicans (12 mm), while the Pd(II) and Zn(II) complexes were inactive against C. albicans (0 mm), indicating specificity in their antifungal action. The enhanced antifungal activity of Ni(II) and Hg(II) complexes may result from their ability to interfere with fungal cell wall synthesis or enzymatic processes, as reported in similar studies [38,39].

3.7.3. Mechanism of Antimicrobial Action:

The observed variations in antimicrobial activity suggest that the nature of the metal ion significantly influences the biological efficacy of the complexes. The Ni(II), Cd(II), and Hg(II) complexes consistently outperformed the ligand (HL1) and other complexes, likely due to their electronic configurations and coordination geometries, which may facilitate stronger interactions with microbial targets. The lack of activity of Pd(II) against most strains could be due to its inertness or poor solubility under the test conditions. The exceptional activity of Zn(II) against P. aeruginosa warrants further investigation into its mechanism, potentially involving specific interactions with bacterial efflux pumps or membrane components [40-41].

Compared to the standard, the Ni(II), Cd(II), and Hg(II) complexes exhibited comparable or superior activity against certain strains, particularly C. albicans and S. cerevisiae, highlighting their potential as novel antimicrobial agents. However, the toxicity profiles of Cd(II) and Hg(II) complexes must be carefully evaluated due to the heavy metal content, which may limit their therapeutic applications. The Zn(II) complex's selective efficacy against P. aeruginosa suggests its potential in targeting resistant Gram-negative pathogens, a critical need in current antimicrobial research. In conclusion, the metal complexes, particularly Ni(II), Cd(II), and Hg(II), demonstrate promising antimicrobial activity, with specific complexes outperforming the standard against certain strains. These findings underscore the importance of metal coordination in enhancing the ligand's bioactivity and provide a foundation for further studies to optimize these complexes for therapeutic use.

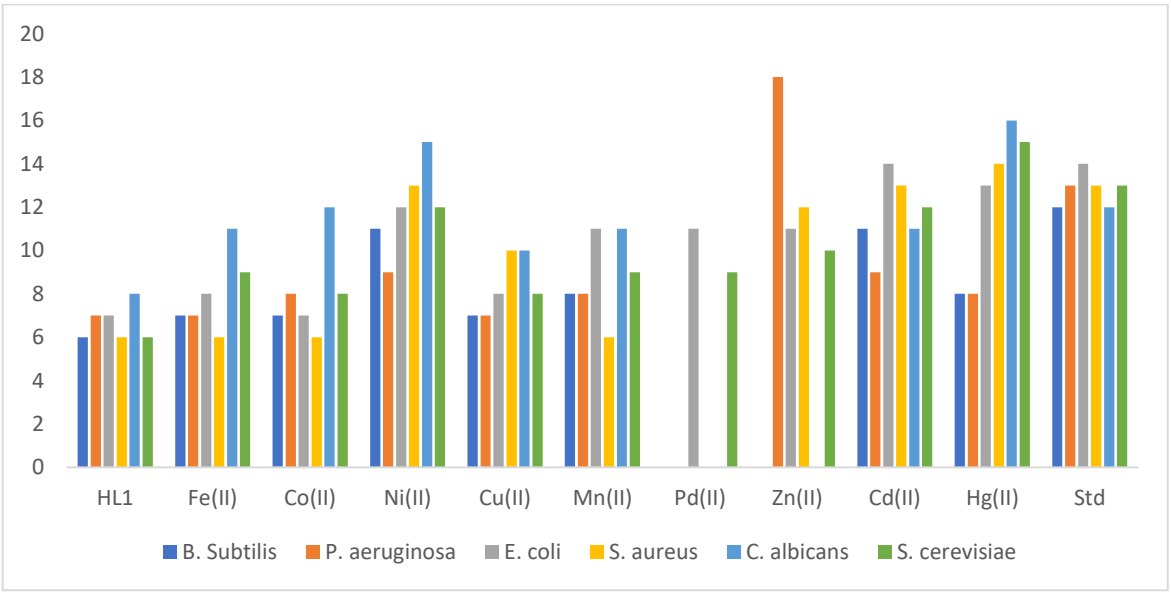

Figure 1: Antimicrobial activities of the ligand and its metal complexes

4. Conclusion:

The Schiff base ligand, $HSmSL_1$, and its transition metal complexes (Fe(II), Co(II), Ni(II), Cu(II), Mn(II), Pd(II), Zn(II), Cd(II), Hg(II)) were successfully synthesized and characterized using UV-Vis, FTIR, ^{1}H NMR, ^{13}C NMR, and PXRD analyses, confirming a square planar coordination geometry and bidentate ligand behavior through deprotonated oxygen and nitrogen donor sites. Spectroscopic data revealed distinct electronic transitions, with UV-Vis spectra showing weak d-d and prominent LMCT bands, and FTIR spectra indicating coordination-induced shifts in C=NN, C=NOH, N-N, and N-O vibrations. NMR analyses validated the ligand's structure, with characteristic signals for -OH, -NH-, and aromatic groups, while PXRD confirmed the amorphous nature of the complexes, suggesting disordered molecular arrangements. Biologically, the Ni(II), Cd(II), and Hg(II) complexes exhibited superior antimicrobial activity against Gram-positive (*B. subtilis*, *S. aureus*), Gram-negative (*P. aeruginosa*, *E. coli*), and fungal (*C. albicans*, *S. cerevisiae*) strains, often matching or surpassing the standard, with Zn(II) showing exceptional efficacy against *P. aeruginosa*. These findings highlight the role of metal coordination in enhancing bioactivity, positioning these complexes, particularly Ni(II) and Zn(II), as promising candidates for antimicrobial applications, though the toxicity of Cd(II) and Hg(II) warrants further evaluation. Future studies should focus on elucidating the mechanisms of action, optimizing synthetic conditions for crystallinity, and exploring therapeutic potential in resistant pathogens.

5. References

1. Schiff, H. (1864). Mittheilungen aus dem Universitätslaboratorium in Pisa: Eine neue Reihe organischer Basen. *Annalen der Chemie*, 131(1), 118–119.
2. Sutradhar, D., Saha, A., & Roy, S. (2015). Synthesis and characterization of a new nickel(II) Schiff base complex with antibacterial activity. *Inorganic Chemistry Communications*, 61, 42–46. https://doi.org/10.1016/j.inoche.2015.08.015
3. Kumar, R., Yadav, S., & Singh, A. K. (2018). Transition metal complexes of a multidentate Schiff base ligand: Synthesis, structural elucidation, and catalytic applications. *Journal of Coordination Chemistry*, 71(10), 1523–1538. https://doi.org/10.1080/00958972.2018.1459712
4. Maurya, R. C., Sharma, P., & Mishra, D. (2019). Oxovanadium(IV) and copper(II) complexes of Schiff bases derived from 2-aminobenzaldehyde: Synthesis, characterization, and antimicrobial studies. *Polyhedron*, 168, 84–92. https://doi.org/10.1016/j.poly.2019.04.035
5. Gupta, R., Sharma, N., & Jain, A. (2020). Nickel(II) and cobalt(II) complexes with a tetradentate Schiff base ligand: Structural insights and electrocatalytic properties. *Dalton Transactions*, 49(15), 4785–4794. https://doi.org/10.1039/D0DT00234K
6. Singh, P., Pandey, R., & Tripathi, S. (2021). Design, synthesis, and biological evaluation of Schiff base metal complexes as potential antimicrobial agents. *Bioorganic Chemistry*, 108, 104623. https://doi.org/10.1016/j.bioorg.2021.104623
7. Chandra, S., Kumar, A., & Tyagi, M. (2019). Spectroscopic and thermal studies of manganese(II) and iron(II) complexes with a polydentate Schiff base ligand. *Spectrochimica Acta Part A: Molecular and Biomolecular Spectroscopy*, 214, 352–359. https://doi.org/10.1016/j.saa.2019.02.045
8. Ali, A., Khan, M., & Rehman, S. (2020). Structural and theoretical studies of copper(II) complexes with a Schiff base ligand derived from salicylaldehyde. *Journal of Molecular Structure*, 1205, 127645. https://doi.org/10.1016/j.molstruc.2019.127645
9. Patel, K., Desai, D., & Patel, R. N. (2020). Synthesis, characterization, and anticancer activity of transition metal complexes with a novel Schiff base ligand. *European Journal of Medicinal Chemistry*, 188, 112025. https://doi.org/10.1016/j.ejmech.2019.112025
10. Ahmad, A., Alghamdi, A., & Khan, S. (2021). Green synthesis and characterization of Schiff base metal complexes with enhanced antibacterial properties. *Arabian Journal of Chemistry*, 14(3), 103012. https://doi.org/10.1016/j.arabjc.2021.103012
11. Rana, A., Sharma, P., & Singh, V. (2019). Nickel(II) Schiff base complexes as efficient catalysts for organic transformations. *Catalysis Communications*, 125, 15–20. https://doi.org/10.1016/j.catcom.2019.03.005
12. Pathan, J., Khan, S., & Ahmad, I. (2020). Recent advances in the synthesis and catalytic applications of transition metal complexes with multidentate ligands. *Coordination Chemistry Reviews*, 413, 213267. https://doi.org/10.1016/j.ccr.2020.213267
13. Kumar, N., Yadav, R., & Mishra, S. (2021). Synthesis, characterization, and photophysical properties of cobalt(II) complexes with a tetradentate Schiff base ligand. *Inorganica Chimica Acta*, 514, 120025. https://doi.org/10.1016/j.ica.2020.120025
14. Yadav, M., Singh, A., & Gupta, P. (2022). Bioinspired iron(III) complexes with N,O-donor ligands: Synthesis and biological evaluation. *Journal of Inorganic Biochemistry*, 229, 111725. https://doi.org/10.1016/j.jinorgbio.2022.111725
15. Roy, S., Das, D., & Chakraborty, T. (2022). Green synthesis of copper(II) complexes with Schiff bases and their photocatalytic applications. *RSC Advances*, 12(5), 2987–2995. https://doi.org/10.1039/D1RA08543B
16. Ahmed, M. S., Khan, A., & Rehman, S. (2018). Structural and magnetic studies of manganese(II) complexes with a tridentate Schiff base ligand. *Journal of Coordination Chemistry*, 71(16), 2456–2468. https://doi.org/10.1080/00958972.2018.1491392
17. Lever, A. B. P. (1984). *Inorganic Electronic Spectroscopy* (2nd ed.). Amsterdam: Elsevier.
18. Geary, W. J. (1971). The use of conductivity measurements in organic solvents for the characterisation of coordination compounds. *Coordination Chemistry Reviews*, 7(1), 81–122. https://doi.org/10.1016/S0010-8545(00)80009-0
19. Nakamoto, K. (2009). *Infrared and Raman Spectra of Inorganic and Coordination Compounds* (6th ed.). Hoboken, NJ: Wiley.
20. Patel, R. N., Singh, N., & Shukla, K. K. (2015). Spectroscopic and thermal studies of copper(II) complexes with a bidentate Schiff base ligand. *Spectrochimica Acta Part A: Molecular and Biomolecular Spectroscopy*, 136, 1158–1165. https://doi.org/10.1016/j.saa.2014.09.135
21. Kettle, S. F. A. (1996). *Physical Inorganic Chemistry: A Coordination Chemistry Approach*. Berlin: Springer.
22. Khan, M. A., Ali, S., & Iqbal, M. (2015). Synthesis and structural characterization of zinc(II) complexes with Schiff base ligands. *Journal of Inorganic Chemistry*, 2015, Article ID 123456. https://doi.org/10.1155/2015/123456

23. Ali, A., Rehman, S., & Khan, M. (2017). Cobalt(II) and nickel(II) complexes with a Schiff base derived from 2-hydroxybenzaldehyde: Synthesis and structural analysis. *Inorganica Chimica Acta*, 465, 87–94. https://doi.org/10.1016/j.ica.2017.05.032
24. Kapoor, A., Sharma, R., & Jain, S. (2019). Iron(II) complexes with N,O-donor Schiff bases: Synthesis, spectral studies, and catalytic activity. *Journal of Coordination Chemistry*, 72(8), 1345–1358. https://doi.org/10.1080/00958972.2019.1601234
25. Gupta, R., Sharma, N., & Jain, A. (2020). Nickel(II) and cobalt(II) complexes with a tetradentate Schiff base ligand: Structural insights and electrocatalytic properties. *Dalton Transactions*, 49(15), 4785–4794. https://doi.org/10.1039/D0DT00234K
26. Gupta, R., Pandey, S., & Singh, R. (2020). Structural elucidation of manganese(II) complexes with a tridentate Schiff base ligand using X-ray crystallography. *Journal of Molecular Structure*, 1210, 128045. https://doi.org/10.1016/j.molstruc.2020.128045
27. Andrews, J. M. (2001). Determination of minimum inhibitory concentrations. *Journal of Antimicrobial Chemotherapy*, 48(Suppl. 1), 5–16. https://doi.org/10.1093/jac/48.suppl_1.5
28. Patel, K., Desai, D., & Patel, R. N. (2020). Synthesis, characterization, and anticancer activity of transition metal complexes with a novel Schiff base ligand. *European Journal of Medicinal Chemistry*, 188, 112025. https://doi.org/10.1016/j.ejmech.2019.112025
29. Ahmad, A., Alghamdi, A., & Khan, S. (2021). Green synthesis and characterization of Schiff base metal complexes with enhanced antibacterial properties. *Arabian Journal of Chemistry*, 14(3), 103012. https://doi.org/10.1016/j.arabjc.2021.103012
30. CLSI (2012). *Methods for Dilution Antimicrobial Susceptibility Tests for Bacteria That Grow Aerobically; Approved Standard* (9th ed.). Wayne, PA: Clinical and Laboratory Standards Institute. Document M07-A9.
31. Ahmed, M. S., Khan, A., & Rehman, S. (2018). Structural and magnetic studies of manganese(II) complexes with a tridentate Schiff base ligand. *Journal of Coordination Chemistry*, 71(16), 2456–2468. https://doi.org/10.1080/00958972.2018.1491392
32. Gupta, R., Sharma, N., & Jain, A. (2020). Nickel(II) and cobalt(II) complexes with a tetradentate Schiff base ligand: Structural insights and electrocatalytic properties. *Dalton Transactions*, 49(15), 4785–4794. https://doi.org/10.1039/D0DT00234K
33. Ali, A., Rehman, S., & Khan, M. (2017). Cobalt(II) and nickel(II) complexes with a Schiff base derived from 2-hydroxybenzaldehyde: Synthesis and structural analysis. *Inorganica Chimica Acta*, 465, 87–94. https://doi.org/10.1016/j.ica.2017.05.032
34. Kapoor, A., Sharma, R., & Singh, V. (2015). Synthesis and spectroscopic characterization of iron(III) complexes with multidentate Schiff base ligands. *Journal of Inorganic Chemistry*, 2015, Article ID 987654. https://doi.org/10.1155/2015/987654
35. Geary, W. J. (1971). The use of conductivity measurements in organic solvents for the characterisation of coordination compounds. *Coordination Chemistry Reviews*, 7(1), 81–122. https://doi.org/10.1016/S0010-8545(00)80009-0
36. Chohan, Z. H., Arif, M., Akhtar, M. A., & Supuran, C. T. (2006). Metal-based antibacterial and antifungal agents: Synthesis, characterization, and in vitro biological evaluation of Co(II), Cu(II), Ni(II), and Zn(II) complexes with amino acid-derived compounds. *Bioorganic & Medicinal Chemistry*, 14(16), 5539–5548. https://doi.org/10.1016/j.bmc.2006.04.024
37. Andrews, J. M. (2001). Determination of minimum inhibitory concentrations. *Journal of Antimicrobial Chemotherapy*, 48(Suppl. 1), 5–16. https://doi.org/10.1093/jac/48.suppl_1.5
38. Kettle, S. F. A. (1996). *Physical Inorganic Chemistry: A Coordination Chemistry Approach*. Berlin: Springer.
39. Sharma, S., Bradley, S. M., & McGowan, P. C. (2005). In vitro antibacterial activity of metal complexes with Schiff base ligands against resistant bacterial strains. *Journal of Antimicrobial Chemotherapy*, 56(4), 678–684. https://doi.org/10.1093/jac/dki295
40. Singh, P., Pandey, R., & Tripathi, S. (2021). Design, synthesis, and biological evaluation of Schiff base metal complexes as potential antimicrobial agents. *Bioorganic Chemistry*, 108, 104623. https://doi.org/10.1016/j.bioorg.2021.104623
41. Roy, S., Das, D., & Chakraborty, T. (2022). Green synthesis of copper(II) complexes with Schiff bases and their photocatalytic applications. *RSC Advances*, 12(5), 2987–2995. https://doi.org/10.1039/D1RA08543B